Archives of Biochemistry and Biophysics 495 (2010) 165–173

Contents lists available at ScienceDirect

Archives of Biochemistry and Biophysics

journal homepage: www.elsevier.com/locate/yabbi

Original paper

Mutations in salt-bridging residues at the interface of the core and lid domains of epoxide hydrolase StEH1 affect regioselectivity, protein stability and hysteresis

Diana Lindberg, Shabbir Ahmad, Mikael Widersten *

Department of Biochemistry and Organic Chemistry, Uppsala University, Box 576, SE-751 23 Uppsala, Sweden

ARTICLE INFO

Article history:
Received 24 November 2009
and in revised form 18 December 2009
Available online 15 January 2010

Keywords:
Epoxide hydrolase
Salt-bridges
Hysteresis
Mutagenesis
Substrate specificity

ABSTRACT

Epoxide hydrolase, StEH1, shows hysteretic behavior in the catalyzed hydrolysis of *trans*-2-methylstyrene oxide (2-MeSO)[1]. Linkage between protein structure dynamics and catalytic function was probed in mutant enzymes in which surface-located salt-bridging residues were substituted. Salt-bridges at the interface of the α/β-hydrolase fold core and lid domains, as well as between residues in the lid domain, between Lys^{179}-Asp^{202}, Glu^{215}-Arg^{41} and Arg^{236}-Glu^{165} were disrupted by mutations, K179Q, E215Q, R236K and R236Q. All mutants displayed enzyme activity with styrene oxide (SO) and 2-MeSO when assayed at 30 °C. Disruption of salt-bridges altered the rates for isomerization between distinct Michaelis complexes, with (1*R*,2*R*)-2-MeSO as substrate, presumably as a result of increased dynamics of involved protein segments. Another indication of increased flexibility was a lowered thermostability in all mutants. We propose that the alterations to regioselectivity in these mutants derive from an increased mobility in protein segments otherwise stabilized by salt bridging interactions.

Introduction

Structure dynamics is an inherent component of enzyme catalysis and is a hallmark of allosteric enzymes [1–5]. We have previously reported that a plant epoxide hydrolase, StEH1 from *Solanum tuberosum*, exhibits hysteretic kinetics [6,7] during the pre-steady state phase of the catalyzed hydrolysis of *trans*-2-methylstyrene oxide (2-MeSO) (Fig. 1) implying that this enzyme is present in different conformations in the substrate-free state [8].

The tertiary structure of StEH1 consists of a canonical α/β-hydrolase fold core domain roofed by a lid domain [9,10] with the active-site situated in a cleft between these two domains and catalytic groups being contributed from both domains (Fig. 2A) [11,12]. The catalytic mechanism involves a covalent enzyme-bound intermediate formed after nucleophilic attack by an enzyme-contributed carboxylate on one of the oxirane carbons so forming a covalent ester intermediate. The reaction is concluded by base-catalyzed hydrolysis of the alkylenzyme to the vicinal diol product [13–17].

The hysteretic behavior of StEH1 is manifested in the transient state reaction kinetics as a decrease in the observed rate of alkylenzyme formation at increasing substrate concentrations [8], and can be modeled by the kinetic mechanism in Scheme 1.

The mechanism invokes that the substrate-free enzyme exists in two different states, E and E′, with distinct substrate-binding properties. In addition, conformational transitions between the different Michaelis complexes (ES and E′S) are included. The model mechanism in Scheme 1 explains the slow transitions detectable in the pre-steady state kinetics and also describes how two different diol products, as observed with (1*R*,2*R*)-2-MeSO as substrate, may be formed (Fig. 1). Similar kinetic mechanisms have been proposed for other α/β-hydrolase fold enzymes: butylcholine esterase [18] and acetylcholine esterase [19].

The structural basis for the difference between E and E′ is unknown and crystal structures of wild-type and mutant enzyme forms have not provided information of possible structural flexibility; the available structures are virtually identical within the experimental error [11,12]. It is possible, however, that the structural differences may escape detection in the X-ray crystallographic experiments either from being too small for detection at the achieved resolution or that one conformer predominates at equilibrium.

Interactions at the interface between the core and lid domains are expected to influence the fine structure and dynamics of the active-site. From the available 3-D structures, a number of salt-bridges can be identified, either connecting the different domains, or present as intra-domain interactions (Fig. 2). The amino acid residues participating in the different interaction networks are relatively well conserved in related plant proteins which may further suggest potential roles for these interactions (Fig. 3).

* Corresponding author. Fax: +46 (0) 18 55 8431.
E-mail address: mikael.widersten@biorg.uu.se (M. Widersten).

[1] *Abbreviations used:* SO, styrene oxide; 2-MeSO, *trans*-2-methylstyrene oxide.

0003-9861/$ - see front matter © 2010 Elsevier Inc. All rights reserved.
doi:10.1016/j.abb.2010.01.007

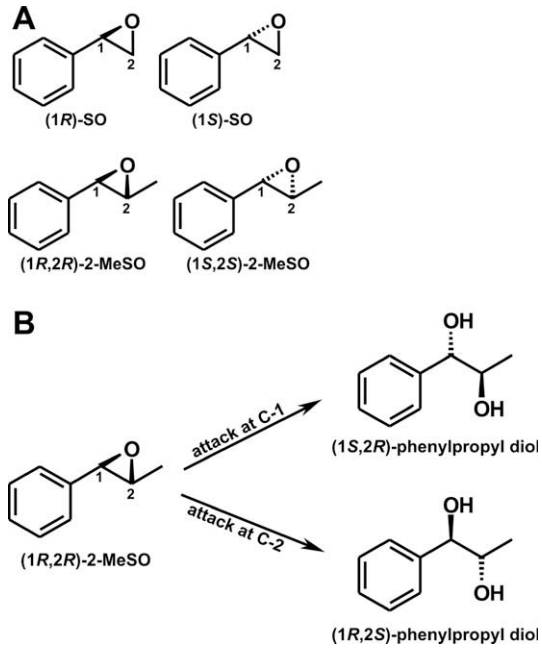

Fig. 1. (A) Epoxide hydrolase substrates studied. (B) Outcome of hydrolysis of (1*R*,2*R*)-2-MeSO resulting from nucleophilic attack at either the benzylic (C-1) or the aliphatic carbon (C-2).

The object of the current work was to analyze the contribution of salt-bridges, located at the enzyme domain interface and within the lid domain, to protein stabilization and, as an extension, their influence on structure dynamics reflected in the enzyme kinetics. Site-directed mutagenesis targeted to destabilize salt-bridge and hydrogen bonding interactions was performed and the mutant enzymes were analyzed for their catalytic and kinetic properties and for thermal stability.

Materials and methods

Chemicals, reagents and bacterial strains

Epoxide substrates were purchased from Sigma–Aldrich at highest purity available. Enantiomeric purity was analyzed by chiral HPLC. Oligonucleotides were custom-made by Thermo Scientific, restriction and DNA modifying enzymes supplied by Fermentas and Promega Corp. *Escherichia coli* XL1-Blue was supplied by Stratagene. Chromatographic resins were purchased from GE Healthcare.

Enzyme mutagenesis

Site-directed mutagenesis was performed by polymerase chain reactions using mutagenic primers and plasmid pGTacStEH1-5H, encoding wild-type StEH1 [17], as template. Sequences of mutagenic oligonucleotides and deduced codon replacements are given in Table 1. Mutated cDNA fragments were subcloned between the *Mun*I and *Sac*I (K179Q, R236K and R236Q) or the *Xho*I and *Sac*I (E215Q) restriction sites of pGTacStEH1-5H. All mutated cDNA inserts were sequenced in full to confirm expected mutations and exclude other alterations.

Sequence alignment

The primary structure of StEH1 was used as query in a BLASTP search of the plant sequence database at Expasy (http://www.expasy.ch/tools/blast/). Hits representing bona fide or inferred epoxide hydrolases from different species were picked and aligned to the StEH1 sequence with ClustalW [20].

Protein expression and purification

Mutated cDNAs were subcloned into pGTacStEH1-5H and purified by Ni(II)-IMAC and size exclusion chromatography as described previously [17]. Enzyme concentrations were determined from UV absorbance spectra of homogeneous proteins in buffer.

Steady state kinetics

Kinetic parameters were determined from the initial rates of enzyme-catalyzed hydrolysis of both enantiomers of styrene oxide (SO) and *trans*-2-methylstyrene oxide (2-MeSO) in the presence of wild-type or mutant StEH1. Initial rates were measured in 0.1 M sodium phosphate, pH 7.5, at 30 °C. Substrates were dissolved in acetonitrile and diluted in buffer so that the final concentration of acetonitrile in the reaction mixtures became 1% (v/v) and substrate concentrations varied in a range of 0.02–0.50 mM. Enzyme concentrations were 20 nM in the reactions with (1*S*)-SO and (1*S*,2*S*)-MeSO and 0.20–0.35 μM in the (1*R*)-SO and (1*R*,2*R*)-MeSO reactions. Epoxide hydrolysis was followed by recording the decrease in absorbance at 225 nm, $\Delta\varepsilon = -2.75$ and $-4.3\ \mathrm{mM^{-1}\ cm^{-1}}$ for SO and 2-MeSO, respectively. Kinetic parameters k_{cat}, K_M and k_{cat}/K_M were determined after fitting the Michaelis–Menten equation using MMFIT and RFFIT in SIMFIT (http://www.simfit.man.ac.uk) to the experimental data. Due to the practically feasible upper substrate concentration limit, the values of k_{cat} and K_M were in some substrate/enzyme combinations determined after extrapolation to saturating conditions, and hence, less well determined. The k_{cat}/K_M parameters were in all cases well determined.

Pre-steady state kinetics

In order to determine microscopic rate constants the catalyzed hydrolysis of the 2-MeSO enantiomers was followed during the pre-steady state phase. Formation of the alkylenzyme intermediate was detected as a concomitant decrease in intrinsic tryptophan fluorescence of the enzyme [21]. Measurements were performed in a sequential stopped-flow spectrophotometer (Applied Photophysics SX.20MV) with an excitation wavelength of 290 nm and detecting fluorescent light collected through a 320 nm cut-off filter. Reactions were performed at 30 °C in 0.1 M sodium phosphate, pH 7.5. Substrate concentrations ranged between 25–1200, or 85–1200 μM, with (1*S*,2*S*)- or (1*R*,2*R*)-2-MeSO, respectively. Enzyme concentrations were 2 or 10 μM with the (1*S*,2*S*)- or (1*R*,2*R*)-2-MeSO respectively. Depending on the level of complexity of the catalyzed reactions, apparent rate constants (k_{obs}) were determined by fitting single (Eq. (1)) or double (Eq. (2)) exponential functions with floating endpoints to averaged (8–12 traces) progression curves. *F* is the fluorescence signal, *A*, the initial fluorescence value at $t = 0$, k_{obs} is the apparent rate constants and *C*, the end point. *F*-tests were performed to validate the use of the higher order equation.

$$F\ (t) = A\ \exp\ (-k_{obs}t) + C \tag{1}$$

$$F\ (t) = A_1\ \exp\ (-k_{obs1}t) + A_2\ \exp\ (-k_{obs2}t) + C \tag{2}$$

When the apparent rates displayed a hyperbolic dependence on substrate concentration, indicative of a mechanism as depicted in Scheme 2, Eq. (3) was fitted to the data. Applying this equation assumes rapid pre-equilibrium of association and dissociation of ES; $[ES] = [S]/(K_S + [S])$. Curve-fitting allows for determination of rate constants for alkylenzyme formation, k_2, and decomposition, k_{-2} and k_3, and the ES dissociation constant, K_S.

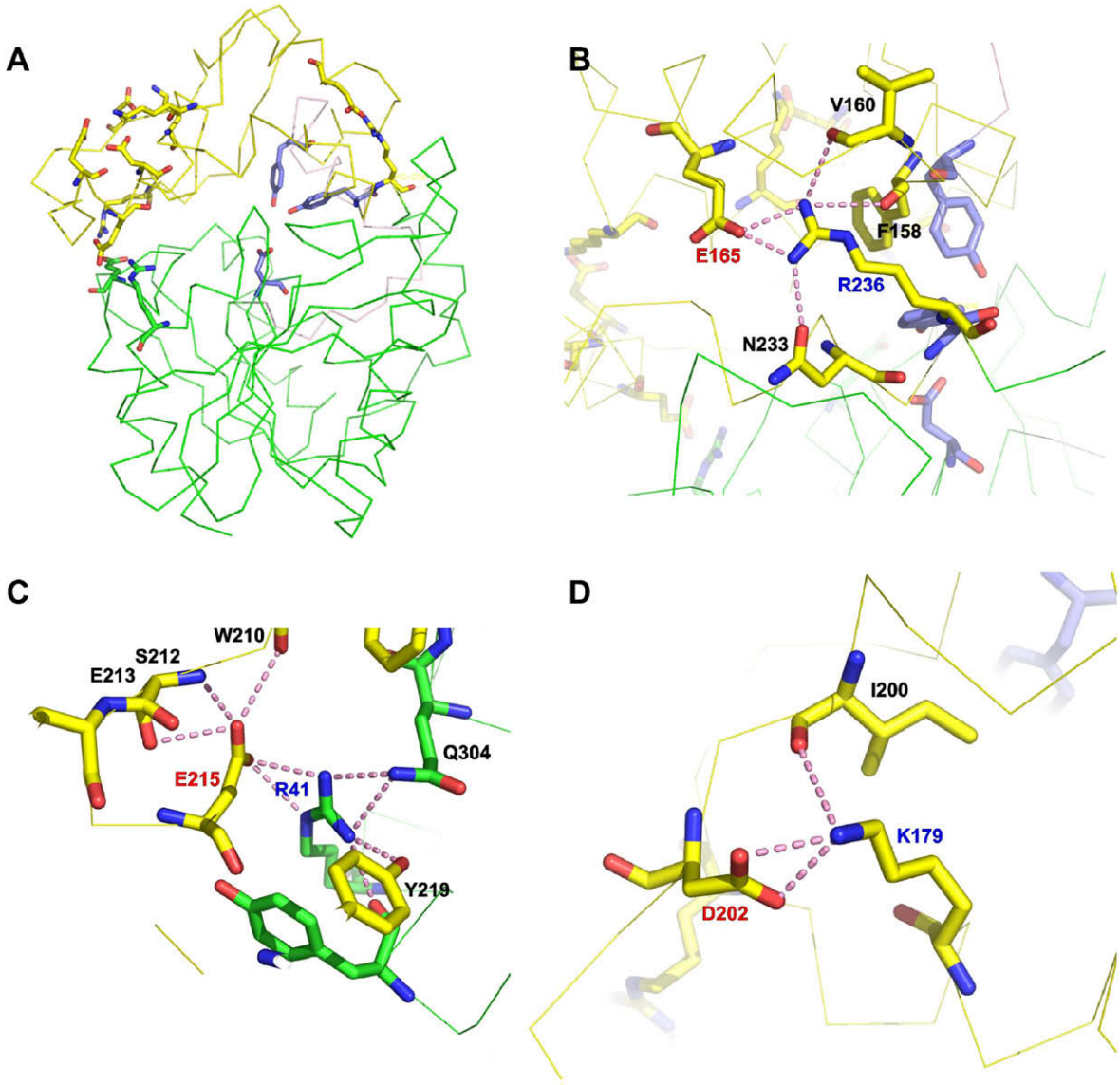

Fig. 2. Salt-bridges at the interface of the core and lid domains of StEH1. (A) Overview of the StEH1 structure with the canonical α/β-hydrolase folded core domain shown in green. The mainly alpha-helical lid domain is colored in yellow. Residues in purple stick representation, two Tyr residues and an Asp, contribute catalytic groups and are included to mark the active-site location. Residues in yellow or green stick representation are involved in charged polar interactions. (B) Arg^{236} is located at the junction between the core and lid domains of StEH1 and adjacent to one of the catalytic Tyr residues (Tyr^{235}). This residue forms a salt-bridge with Glu^{165} and hydrogen bonds with main- and side-chain groups of nearby residues. (C) Glu^{215} and Arg^{41} interact through an inter-domain salt-bridge and via a number of hydrogen bonds with side- and main-chain groups of nearby residues from both domains of the protein. (D) Salt-bridge involving Asp^{202} and Lys^{179}. The Lys residue also interacts with the backbone carbonyl of Ile^{200}. Image created using the atomic coordinates in 2cjp [11] with PyMOL (DeLano Scientific; www.pymol.org).

When the apparent rates displayed a negative dependence on substrate concentration, a situation described in Scheme 1 involving rate-limiting hysteretic steps, Eq. (4) was fitted to the data which is a rewritten form of Eq. (5), the rate law for the kinetic mechanism in Scheme 1 [18]. This fit does not allow for determination of individual rate constants but provides the sum of the rates of interconversion of the ES⇄E′S ($k_5 + k_{-5}$) as determined by the end-point rate at saturating [S].

$$k_{obs} = \frac{k_2[S]}{K_S + [S]} + (k_{-2} + k_3) \tag{3}$$

$$k_{obs} = \frac{K_S K'_S(k_0 + k_{-0}) + [S]\left[K_S(K_0 + k_{-5}) + K'_S(K_{-0} + k_5)\right] + [S]^2(k_5 + k_{-5})}{K_S K'_S + [S](K_S + K'_S) + [S]^2} \tag{4}$$

$$k_{obs} = \frac{k_0 + (k_5/K_S)[S]}{1 + ([S]/K_S)} + \frac{k_{-0} + (k_{-5}/K'_S)[S]}{1 + ([S]/K'_S)} \tag{5}$$

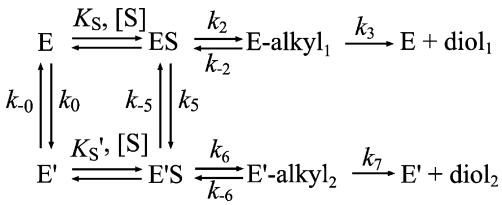

Scheme 1.

Thermostability of enzyme activity

To investigate thermostability of mutants and wild-type StEH1, enzyme activity was measured after incubation for different time periods at three different temperatures: 30, 45 and 55 °C. The activity was measured spectrophotometrically at 225 nm, by observing the decrease in absorbance due to hydrolysis of epoxides

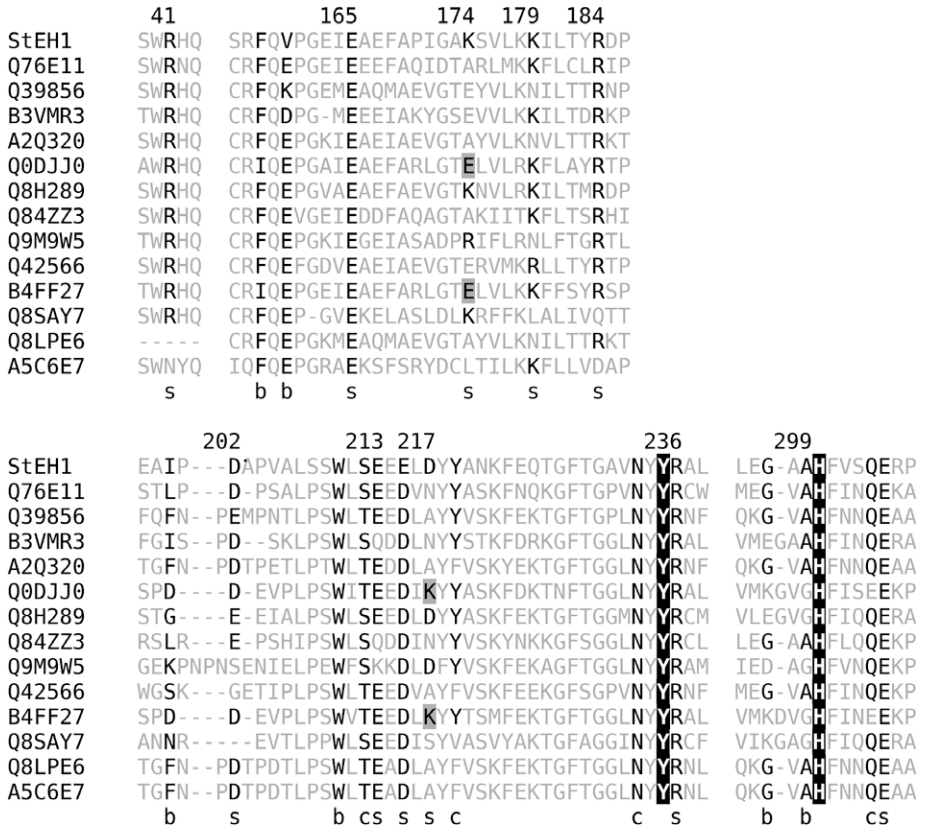

Fig. 3. Sequence alignment of plant epoxide hydrolases. Residues in black are involved in salt-bridge or hydrogen bond interactions at the lid and core domain interface of StEH1. s, salt-bridge interaction; b, hydrogen bond through backbone peptide group; c, hydrogen bond involving side-chain functional group. The catalytic residues Tyr^{235} and His^{300} are shown in white on black. Black letters on gray indicates positions of possible compensatory mutations preserving the ability to form ionic interactions. Q76E11, *Citrus jambhiri* [41], Q39856, *Glycine max* [42], B3VMR3, *Nicotiana benthamiana* [accession EU779658], A2Q320, *Medicago truncatula* [accession AC154391], Q0DJJ0, *Oryza sativa* subsp. *japonica*, [43], Q8H289, *Ananas comosus* [44], Q84ZZ3, *Euphorbia lagascae* [45], Q9M9W5, *Arabidopsis thaliana* [accession AC011620], Q42566, *Arabidopsis thaliana* [46], B4FF27, *Zea mays* [accession BT035715], Q8SAY7, *Oryza sativa* [accession AC096687], Q8LPE6, *Cicer arietinum* [accession AJ487037], A5C6E7, *Vitis vinifera* [47].

Table 1
Oligonucleotide sequences of mutagenic primers[a,b].

Name	Sequence (5′–3′)	Codon change
K179Q	TTG CTC *CAA TTG* GTG CTA AGT CTG TTC TTA AG**C** AAA TAT TGA CAT ACC GCG ATC	AAA to CAA
E215Q-1	CTT GTT GGC ATA GTA ATC CAA CTG TTC CT**C** AGA AAG CCA CGA TG	GAG to CAG
E215Q-2	GTT GGA TTA CTA TGC CAA CAA G	–
R236KQ	TAA CTT *GAG CTC* CTG TCC ATG GTG CTG TGA GTT CCC AGT TTA TGG GTA AAG C**CT K**GTAAT AGT TAA CTG CAC CAG T, K = T/G	CGT to AAG/CAG

[a] Italicized letters: restriction endonuclease recognition sites.
[b] Bold letters: nucleotide replacements.

$$E + S \underset{}{\overset{K_S}{\rightleftharpoons}} ES \underset{k_{-2}}{\overset{k_2}{\rightleftharpoons}} E\text{-alkyl} \xrightarrow{k_3} E + \text{diol}$$

Scheme 2.

to diol, in 0.1 M sodium phosphate, pH 7.5, at 30 °C as described above. (1*S*,2*S*)-2-MeSO at 0.30 mM was used as substrate for all StEH1 variants. Enzyme was added to a final concentration of 20 nM. Apparent rate constants of inactivation ($k_{inactive}$) were determined from fitting an equation for single exponential decay to the experimental data (Eq. 6). The half-lives were calculated from $t_{1/2} = \ln 0.5/-k_{inactive}$.

$$\text{Activity}(t) = A \exp(-k_{inactive} t) \quad (6)$$

Regioselectivity

To investigate the regioselectivity of the StEH1 variants, hydrolysis reactions with both enantiomers of 2-MeSO were performed (in triplicates) at 30 °C with continuous agitation for 24 h in the presence of acetonitrile (3% (v/v)), substrate (7.32 mM) and enzyme (2 μM). The reaction volume was adjusted to 500 μl by addition of 0.1 M sodium phosphate, pH 7.5 buffer. After completed hydrolysis, the reaction mixture was evaporated and the diol products were dissolved in the solvent used as mobile phase in the subsequent HPLC separation. Samples were loaded onto a straight phase system and separated over a chiral column (Chiralpak, AS-H, 0.46 cm Ø × 25 cm) with a mobile phase consisting of hexane/isopropanol (93:7). The column was coupled to a Shimadzu Prominence LC-20AD pump and peaks were detected at 220 nm using a Prominence SPD-M20A diode array detector. Molar ratios of diols were determined from the peak areas of the separated reaction products.

Results

Residue selection, mutagenesis, protein expression and purification

Salt-bridging residues were identified from the X-ray crystal structure of StEH1 (Fig. 2). Residues Lys^{179}, Glu^{215} and Arg^{236}, situated at the protein surface were selected for mutation and were replaced by glutamine (K179Q, E215Q and R236Q) or lysine (R236K) residues. Residue replacements were chosen to preserve the polar

character of the protein surface and thereby lowering the risk of adverse effects on protein solubility. The StEH1 mutants were expressed in *E. coli* XL1-Blue and purified to homogeneity by Ni(II)-IMAC chromatography and size exclusion chromatography. Final yields of purified proteins ranged from 8 to 10 mg per liter of batch culture, comparable to purifications of the wild-type enzyme. The purification yield of mutant R236Q, however, was lower (2–5 mg per liter culture) indicating lower stability and/or solubility of this variant. Purified proteins were stored at 4 °C without loss in enzyme activity over the time period of the measurements.

Hysteresis

The hysteretic behavior in the kinetics of StEH1 have been previously established with both 2-MeSO enantiomers as substrates [8]. In all mutants, except for R236Q, the same slow transitions were detected in the pre-steady state phase of the reactions with either 2-MeSO enantiomer (Fig. 4A and C). In the case of the R236Q mutant the transient state kinetics with (1*S*,2*S*)-2-MeSO as substrate could only be modeled according to Scheme 2 and did not display an observed rate that decreased with increasing substrate concentration (Fig. 4). The stopped-flow measurements with (1*R*,2*R*)-2-MeSO as substrate could not be determined with this mutant due to the low protein purification yields.

Enzyme kinetics

When catalytic efficiencies at saturating substrate concentration were determined, it was clear that the mutants in general displayed k_{cat} values lower than the wild-type enzyme (Table 2). The turnover numbers showed a general trend of wild-type > K179Q > E215Q > R236K > R236Q. Pre-steady state kinetics have identified hydrolysis of the alkylenzyme intermediate to be rate-limiting in the wild-type-catalyzed reaction with (1*S*,2*S*)-2-MeSO [8]. This appears to be true also for the salt-bridge mutants as the trend for $k_3^{SS\text{-}2\text{-}MeSO}$ is similar to $k_{cat}^{SS\text{-}2\text{-}MeSO}$ (Tables 2 and 3).

The catalytic efficiencies under non-saturating conditions, as expressed in k_{cat}/K_M, did not follow the same pattern. With (1*R*)-SO, K179Q and E215Q promoted hydrolysis 2 to 2.5-fold more efficiently as compared to the wild-type enzyme (Table 2), while other mutants performed on par with the wild-type. In the (1*S*)-SO reaction, relatively small effects were observed from the mutations with the exception of R236Q which displayed approximately threefold lower activity as compared to the wild-type enzyme. k_{cat}/K_M for hydrolysis of (1*R*,2*R*)-2-MeSO follows the pattern of k_{cat} with this substrate, indicating that chemical turnover is primarily rate-limiting for the enzyme efficiency in this reaction. The largest effect on enzyme efficiencies was observed with (1*S*,2*S*)-2-MeSO. All mutants showed lower activities, with R236Q again as the most affected mutant, displaying 7.5-fold lower catalytic efficiency as compared to the wild-type enzyme.

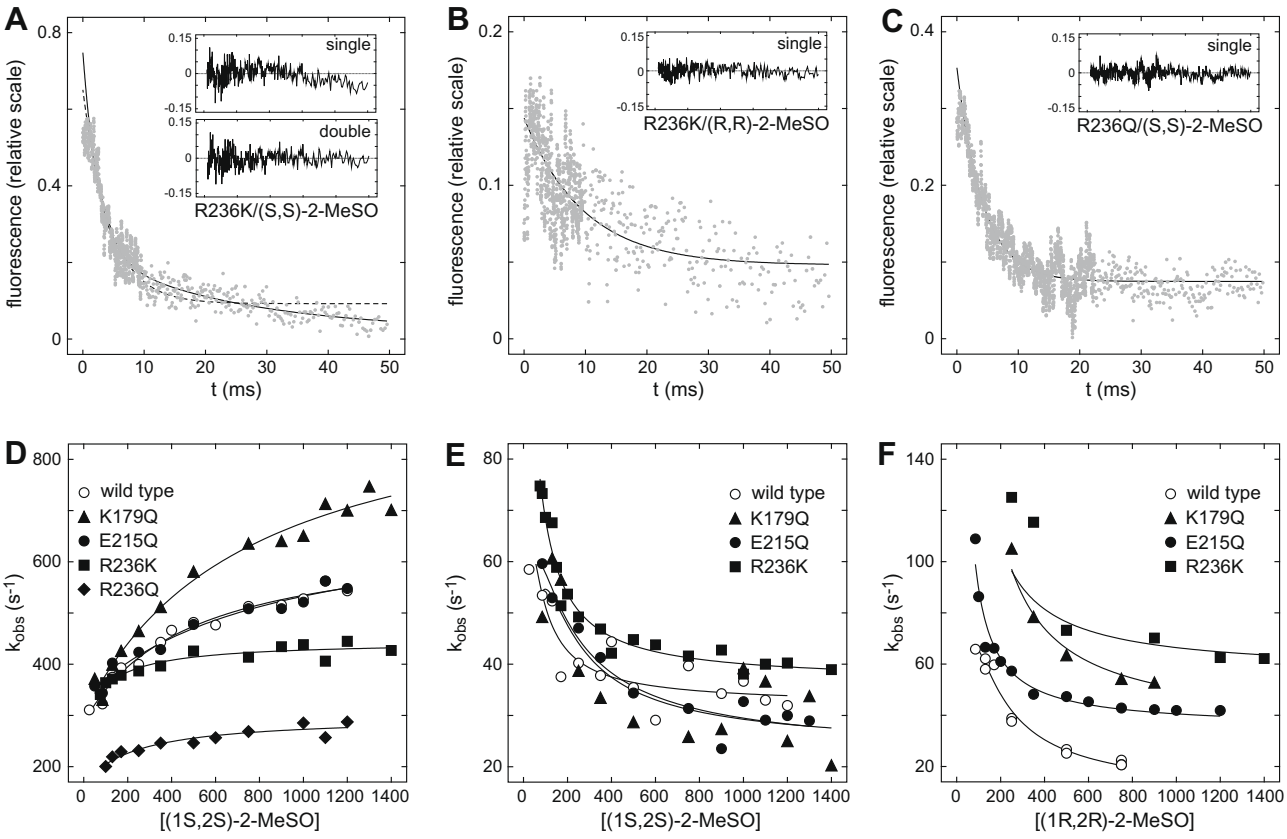

Fig. 4. (A) Typical example of an averaged experimental trace (grey dots) of fluorescence quenching indicative of alkylenzyme formation during the pre-steady state of the reaction with 500 μM (1*S*,2*S*)-2-MeSO and 2 μM R236K mutant. Lines represent fits of single (dashed line) or double (solid line) exponential functions. The double exponential fit provides two observable apparent rates, k_{obs1} and k_{obs2}. Similar traces were recorded for the wild-type, K179Q and the E215Q enzymes with this substrate. Residual plots of the respective fits are shown as inset. (B) As in (A), but with 350 μM (1*R*,2*R*)-2-MeSO as substrate. Solid line represents the fit of a single exponential function. (C) As in (A), but with 2 μM R236Q as catalyst. Solid line represents the fit of a single exponential function. (D–F) Substrate concentration-dependence of k_{obs}. Hyperbolic concentration-dependence was observed for the more rapid apparent rates obtained from the double exponential fit with (1*S*,2*S*)-2-MeSO as substrate and the wild-type, K179Q, E215Q and R236K. The observed rates in the reactions catalyzed by R236Q were obtained from single exponential fits as exemplified in (C). Negative substrate concentration-dependence was observed for the slower observed rates with (1*S*,2*S*)-2-MeSO (E) as well as for the single rate obtained with the (1*R*,2*R*)-enantiomer as substrate (F). See the Materials and methods section for detailed descriptions of fitted equations. Determined parameter values are presented in Table 3.

Table 2
Steady state kinetic parameters of enzyme-catalyzed epoxide hydrolysis in 0.1 M sodium phosphate, pH 7.5, 30 °C.

Enzyme	Substrate													
	(1*R*)-SO			(1*S*)-SO			E[a]	(1*R*,2*R*)-2-MeSO			(1*S*,2*S*)-2-MeSO			E[a]
	k_{cat} (s^{-1})	k_m (mM)	k_{cat}/K_M (s^{-1} mM^{-1})	k_{cat} (s^{-1})	k_m (mM)	k_{cat}/K_M (s^{-1} mM^{-1})	S/R (fold)	k_{cat} (s^{-1})	k_m (mM)	k_{cat}/K_M (s^{-1} mM^{-1})	k_{cat} (s^{-1})	k_m (mM)	k_{cat}/K_M (s^{-1} mM^{-1})	S,S/R,R (fold)
Wild-type	3.3 ± 0.9	3.4 ± 1	0.99 ± 0.03	8.4 ± 0.4	0.12 ± 0.02	68 ± 6	69	4.7 ± 0.7[b]	0.49 ± 0.1[b]	9.7 ± 2[b]	63 ± 3	0.077 ± 0.01	820 ± 100	85
K179Q	2.1 ± 0.6	1.1 ± 0.4	1.9 ± 0.2	7.9 ± 0.3	0.068 ± 0.009	110 ± 10	58	4.0 ± 0.4	0.42 ± 0.08	9.6 ± 0.8	47 ± 1	0.12 ± 0.007	390 ± 20	41
E215Q	2.2 ± 0.4	0.81 ± 0.2	2.6 ± 0.2	5.5 ± 0.3	0.11 ± 0.01	48 ± 4	18	3.0 ± 0.2	0.43 ± 0.04	7.3 ± 0.2	23 ± 0.6	0.044 ± 0.004	590 ± 50	81
R236 K	1.6 ± 0.4	1.8 ± 0.6	0.97 ± 0.06	7.2 ± 0.3	0.14 ± 0.01	58 ± 4	32	1.8 ± 0.2	0.36 ± 0.05	6.1 ± 4	30 ± 2	0.064 ± 0.01	490 ± 80	80
R236Q	0.89 ± 0.2	0.98 ± 0.4	0.86 ± 0.07	4.5 ± 0.4	0.21 ± 0.04	21 ± 2	24	1.2 ± 0.1	0.34 ± 0.05	3.6 ± 0.2	35 ± 2	0.34 ± 0.04	110 ± 6	31

[a] Calculated from $k_{cat}/K_M^S/k_{cat}/K_M^R$.
[b] Values were obtained after fitting the Michaelis–Menten equation. The wild-type enzyme does display a small degree of cooperativity with (1*R*,2*R*)-2-MeSO under these assay conditions which was not taken into consideration here.

In reactions following Scheme 2 (both enantiomers of SO, and in practice (1*S*,2*S*)-2-MeSO [8]) K_M is described by Eq. (7). The value of K_M will decrease as formation and stabilization of ES and alkylenzyme is promoted, i.e. low K_S and high k_2 relative to k_{-2} and k_3.

$$K_M = \frac{K_S\,(k_{-2} + k_3)}{(k_2 + k_{-2} + k_3)} \tag{7}$$

In all mutants, with (1*R*)-SO as substrate, K_M was two to fourfold lower than the wild-type enzyme value, suggesting that enzyme-intermediate complexes are stabilized to a higher degree in these enzyme variants. This may be linked to the slightly lower values of k_{cat} in the mutants indicating slower hydrolysis rates. With (1*S*)-SO and (1*R*,2*R*)-2-MeSO no clear effects on K_M were observed; variations were less than twofold when comparing the different enzyme forms. The case of (1*R*,2*R*)-2-MeSO should be considered special since this reaction is best modeled by the mechanism in Scheme 1. In this case the stabilization and decay of ES, E′S, E-alkyl$_1$ and E-alkyl$_2$ will all contribute to K_M. Hence, compensatory effects may be present precluding differences in stabilization of individual enzyme-intermediate forms. The K_M value for (1*S*,2*S*)-2-MeSO, was relatively unchanged with the exception of the R236Q mutant, which displayed a value more than fourfold higher than the wild-type enzyme, mainly due to a lower alkylation rate (k_2) (Table 3).

Thermostability of enzyme activity

To probe the contribution of salt-bridges to protein structure stability, the wild-type and mutated enzymes were subjected to elevated temperatures followed by activity measurements. All salt-bridge mutations affected thermal stability negatively to different degrees. The most stable mutants K179Q and E215Q displayed half-lives approximately 50-fold shorter than the wild-type enzyme at 55 °C (Table 4). The Arg^{236} mutants were more severely affected with R236Q being the most temperature sensitive.

Regioselectivity

The regioselectivity of (1*R*,2*R*)-2-MeSO hydrolysis is not absolute and the StEH1-catalyzed hydrolysis produces both possible diol products at a certain molar ratio [8]. When diol product ratios were analyzed after complete hydrolysis of (1*S*,2*S*)- or (1*R*,2*R*)-2-MeSO differences were observed between the wild-type and mutant enzymes (Table 5). With (1*S*,2*S*)-2-MeSO the nucleophilic attack occurs almost exclusively at carbon-1. This property appears unaltered by the salt-bridge mutations. The regioselectivity in hydrolysis of (1*R*,2*R*)-2-MeSO, however, was altered to different degrees in the mutants. The relatively low discrimination between the two epoxide carbons shown by the wild-type enzyme was retained in K179Q. E215Q was totally promiscuous while both Arg^{236} mutants displayed substantially higher discrimination favoring attack at carbon-1 and thereby increasing the ee value from 15 to >40% of the (1*S*,2*R*)-diol (Table 5).

Discussion

Due to the chiral nature of epoxides stereospecificity in enzymes acting upon them as substrates will influence catalysis. This includes enantiomer discrimination, and with asymmetric epoxides, regiospecificity of epoxide ring opening. Most epoxide hydrolases that have been examined do exhibit stereoselectivity to different degrees. Although detailed descriptions of the active-site structures of several epoxide hydrolases are available from X-ray crystallographic studies [11,12,22–27] it is yet non-trivial to draw up general descriptions of structural determinants for substrate

Table 3
Pre-steady state kinetic parameters in 0.1 M sodium phosphate, pH 7.5, 30 °C.

Enzyme	Substrate						
	(1*S*,2*S*)-2-MeSO						(1*R*,2*R*)-2-MeSO
	K_S (mM)	k_2 (s^{-1})	k_2/K_S (s^{-1} mM^{-1})	k_{-2} (s^{-1})	k_3 (s^{-1})	($k_5 + k_{-5}$) (s^{-1})	($k_5 + k_{-5}$) (s^{-1})
Wild-type	0.47 ± 0.1	370 ± 20	770 ± 200	170 ± 20	110 ± 10	32 ± 2	8.1 ± 3
K179Q	0.75 ± 0.2	650 ± 50	870 ± 200	230 ± 20	69 ± 7	23 ± 4	56 ± 8
E215Q	0.84 ± 0.4	370 ± 70	440 ± 200	290 ± 20	44 ± 10	22 ± 2	35 ± 2
R236K	0.16 ± 0.1	160 ± 50	1000 ± 700	200 ± 70	83 ± 30	36 ± 1	35 ± 4
R236Q	0.23 ± 0.2	130 ± 20	590 ± 400	85 ± 30	78 ± 20	–	n.d.

Table 4
Time-dependent heat-inactivation of enzyme activity.

Enzyme	$t_{1/2}$ (min)[a] T (°C)		
	30	45	55
Wild-type	>500	>500	53 ± 5
K179Q	>500	>500	1.4 ± 0.3
E215Q	>500	>500	5.0 ± 1
R236K	>500	38 ± 2	1.1 ± 0.4
R236Q	460 ± 100	9.0 ± 0.5	0.31 ± 0.04

[a] Half-life of enzyme activity after incubation at the given temperatures, measured at 30 °C in the presence of 0.3 mM (1*S*,2*S*)-2-MeSQ in 0.1 M sodium phosphate, pH 7.5.

specificity, and to an even lesser extent, stereospecificity. Available descriptions explaining the structure–function relationships behind enantiospecificity in a given enzyme are essentially empirical and has primarily been based on results from experiments in which stereospecificity of epoxide hydrolases has been manipulated by directed evolution [27–31]. If the mutagenesis regime has involved random-site substitutions, amino acid residue alterations augmenting enantiospecificity may in the evolved enzyme be located both near or away from first-sphere substrate-interacting residues [28,29,31]. On the other hand, restricting mutagenesis to first-sphere active-site residues may also generate higher enantiospecificity [30]. A recent report explains the basis for enhanced enantiopreference for the *S*-enantiomer of phenylglycidyl ether in an in vitro-evolved variant of the *A. niger* isoenzyme. In this case, introduction of active-site residues sterically interfering with productive binding of the *R*-enantiomer was responsible for substrate discrimination [27].

Apart from structural restrictions on productive enzyme–substrate interactions, the kinetics of enzyme structure dynamics and of individual catalytic steps will be expressed in observed enantio- and regiospecificities. We recently proposed a model for the kinetic mechanism of epoxide hydrolase StEH1 (Scheme 1) which takes into account promiscuous regioselectivity as well as partially rate-limiting conformational changes in the free enzyme and enzyme–substrate complexes, resulting in hysteretic kinetics [8]. The model adequately explains the enzyme behavior behind the kinetic data obtained both during the pre-steady state and the steady state phases of catalyzed reactions.

StEH1 displays relatively high enantiospecificity for the substrate epoxides SO and 2-MeSO with E-values ranging from 40 to 150 depending on epoxide and pH (Table 2) [8,32]. The distribution of diol products, however, is strongly dependent on the enantiomeric form of epoxide substrate. With SO, StEH1-catalyzed hydrolysis results in enantioconvergence with the (1*R*)-phenylethanediol being formed at high enantiomeric excess [32]. This is due to that regiospecificity is almost totally inverted from attack at the achiral carbon-2 with (1*R*)-SO to reaction at the chiral carbon-1 with the *S*-enantiomer. Hydrolysis of 2-MeSO is more complex with very high regiospecificity for attack at carbon-1 of the (1*S*,2*S*)-enantiomer (ee > 98%), but with lower selectivity with the (1*R*,2*R*)-enantiomer [8]. Furthermore, the steady state kinetics with the latter enantiomer displays cooperativity at lowered assay temperatures [D. Lindberg, M. De La Fuente, M. Widersten, unpublished], indicative of multiple enzyme–substrate complexes which is another hallmark of hysteresis in kinetics [7].

Although there is no evidence from X-ray crystal structures that StEH1 exists in different metastable conformations, productive binding of an asymmetric epoxide would demand a particular active-site structure possessing adequate dynamic properties for catalysis to proceed efficiently. The example of the 2-MeSO enantiomers demonstrates this: hydrolysis of (1*R*,2*R*)-2-MeSO is partially rate-limited by an observed rate that decreases with increasing concentration of substrate, suggesting that structural interconversion between different structural forms of the ES complex exists.

Salt-bridges in folded proteins have been demonstrated to affect protein stability and dynamics [33–36]. Observed effects from replacing salt-bridging residues have been explained as due to loss in direct binding energies in the ionic interactions, changes in free energies of desolvation and changes in overall polar interactions in the folded proteins [37]. In StEH1, a number of such interactions are found (Fig. 2), in some cases located distantly from the catalytic site. The overall effects observed by disturbing these interactions

Table 5
Regioselectivity in hydrolysis of *trans*-2-methylstyrene oxide in 50 mM sodium phosphate, pH 7.5, 30 °C.

Enzyme	Enantiomeric excess of diol products Substrate					
	(1S,2S)-2-MeSO			(1*R*,2*R*)-2-MeSO		
	ee (%)[a]	$\Delta\Delta G^{*}$[b] (kJ/mol)	Major:minor product	ee (%)[a]	$\Delta\Delta G^{*}$[b] (kJ/mol)	Major:minor product
Wild-type	98.2 ± 0.006	−11.8	(1*R*,2*S*):(1*S*,2*R*)	15 ± 4	−0.7	(1*S*,2*R*):(1*R*,2*S*)
K179Q	99.8 ± 0.05	−17.4	(1*R*,2*S*):(1*S*,2*R*)	20 ± 2	−1.0	(1*S*,2*R*):(1*R*,2*S*)
E215Q	99.5 ± 0.2	−14.6	(1*R*,2*S*):(1*S*,2*R*)	1.8 ± 2	−0.09	(1*S*,2*R*):(1*R*,2*S*)
R236K	99.7 ± 0.007	−16.4	(1*R*,2*S*):(1*S*,2*R*)	42 ± 3	−2.3	(1*S*,2*R*):(1*R*,2*S*)
R236Q	99.7 ± 0.02	−16.4	(1*R*,2*S*):(1*S*,2*R*)	44 ± 6	−2.4	(1*S*,2*R*):(1*R*,2*S*)

[a] $(C_{\text{major diol}} - C_{\text{minor diol}})/(C_{\text{major diol}} + C_{\text{minor diol}}) \times 100$.
[b] $\Delta\Delta G^{\ddagger} = -RT\ln$ [major diol]/[minor diol] [40].

through conservative replacements can be summarized as affecting thermostability, hysteretic behavior and regioselectivity.

(1) Arg^{236}-Glu^{165}. This salt-bridge, also involving other residues through hydrogen bonding (Fig. 2B) associates a loop (the "cap-loop" [38]) connecting the core domain, through Arg^{236}, with the lid domain, the "NC-loop" [38]. Arg^{236} is in the linear amino acid sequence adjacent to one of the catalytic tyrosine residues (Tyr^{235}) which suggests a possible stabilizing role of the catalytic site through this salt-bridge. The interaction is highly conserved in other plant enzymes (Fig. 3) further indicating an important structural role.

The anticipated effect of replacing Arg^{236} with Lys was to decrease the valency in hydrogen bonding with Val^{160}, Phe^{158} and Asn^{233}, and to weaken the ionic interaction with Glu^{165}. The resulting mutant is catalytically active with both SO and 2-MeSO, albeit with lower efficiencies as compared to the wild-type enzyme (Table 2). The largest effect by the replacement is observed in the stability at elevated temperatures (Table 4). If the destabilization of the replacement is due to losses in enthalpic bonding energy or unfavorable solvation effects is unknown. Although the efficiencies of catalysis of the different reactions were quite similar to the wild-type enzyme, clear effects could be observed in the pre-steady state phase. With (1*R*,2*R*)-2-MeSO, the sum of the rates for the interconversion between ES and E′S (Scheme 1) shows a higher value demonstrating a more rapid interconversion between these enzyme–substrate complexes (Table 3, Fig. 4F). If the change is in mainly one direction, or in a compensatory manner, is unresolved. The mutation has also affected regiospecificity in this reaction considerably. The preference for nucleophilic attack at carbon-1 is higher in this mutant as compared to the wild-type enzyme. The estimated change in free-energy differences is subtle, however, and corresponds to −1.6 kJ/mol (Table 5). This demonstrates that small alterations to protein dynamics affecting the flux through the different pathways of Scheme 1, directly influence the outcome of product ratios. In the case of (1*S*,2*S*)-2-MeSO, the attack of the enzyme nucleophile is in all cases almost exclusively at carbon-1 and proceeds through a route $E + S \rightarrow ES \rightarrow E\text{-alkyl}_1 \rightarrow E + diol_1$ (Schemes 1 and 2), detected as an observed rate of alkylenzyme formation increasing with substrate concentration (Eq. 3). In addition, a route $E \rightarrow E' \rightarrow E'S \rightarrow ES \rightarrow E\text{-alkyl}_1 \rightarrow E + diol_1$ has to be invoked to explain the slower observed rate which decreases with increasing substrate concentration (Fig. 4E). The enantiomeric excess of the major (1*R*,2*S*)-diol is unaffected (Table 5).

The anticipated effect by the R236Q mutation was to fully remove any ionic interactions and thereby abolish this contribution to the enzyme's structural properties. The R236Q mutant resembles functionally its R236K relative. The enzyme activity is decreased with all substrates, although to a moderate degree (Table 2). The main change is a drastically shortened half-life at elevated temperatures (Table 4), demonstrating a further destabilization of the enzyme structure. In the pre-steady state analysis of the (1*S*,2*S*)-2-MeSO reaction the slower rate observed previously with the wild-type enzyme [8] was absent, with only a single rate detectable (Fig. 4C). This can be interpreted such that structural interconversions in this mutant are more rapid and therefore preventing accumulation of reaction intermediates to detectable levels.

(2) Glu^{215}-Arg^{41}. Glu^{215} is situated at the N-terminal end of one of the lid domain helices forming the cap-loop [38] at the interface with the core domain. One of the carboxylate oxygens (OE2) forms hydrogen bonds with the hydroxyl group and backbone nitrogen of the lid Ser^{212} (Fig. 2C). The other oxygen (OE1) participates in a salt-bridge with the guanidinium group of Arg^{41}, which in turn is hydrogen bonded to the side-chains of Tyr^{219} and Gln^{304}. Glu^{215} is also the terminal residue in a hydrogen-bond chain leading from the hydrolytic water molecule in the active-site to solvent. This chain of interaction has been proposed to function as an exit route for protons generated during catalytic turnover [39]. This salt-bridge interaction appears to be conserved in plant enzymes (Fig. 3). Replacing the carboxylate with an amide in E215Q was expected to break the ionic interaction with Arg^{41} and alter the hydrogen bonding network formed with surrounding groups.

The catalytic efficiency of E215Q was almost threefold higher than the wild-type due to a lower K_M value for (1*R*)-SO. The lower K_M is not likely caused by stronger interactions between enzyme and substrate since the mutated residue is located 18 Å away from the active-site, at the protein surface. Since k_{cat} is virtually unchanged, as compared to the wild-type (Table 2), the K_M-effect is expected to primarily be caused by an increase in the ratio of k_2/k_{-2} leading to accumulation of alkylenzyme. With the exception of a slightly lower $K_M^{(SS)\text{-}2\text{-}MeSO}$, caused by a lower alkylenzyme hydrolysis rate, the E215Q mutant retains as a whole the kinetic properties of the wild-type enzyme. A clear effect from the mutation, however, is the loss in regioselectivity in the hydrolysis of (1*R*,2*R*)-2-MeSO. The E215Q-catalyzed hydrolysis produced an essentially racemic mixture of diol products (Table 5). The sum of the rates of interconversions between ES and E′S was similar to that of R236K which, in contrast to E215Q, displays an increase in preference for attack at carbon-1 of the epoxide (Table 5). Hence, if hysteresis is coupled to regioselectivity it is implied that the changes in the individual values of k_5 and k_{-5} are not equal in the different mutants. The 10-fold shorter half-life at 55 °C reveals that the affected interactions are indeed important to maintain a functional form of the protein (Table 3).

(3) Lys^{179}-Asp^{202}. Lys^{179}, situated in one of the lid helices, is involved in a salt-bridge with Asp^{202} and hydrogen bonded to the backbone carbonyl of Ile^{200} (Fig. 2D). Lys^{179} was replaced by a Gln to remove ionic interactions, yet maintaining the polar nature of the original residue. Since Lys^{179} and Asp^{202} are situated in the same protein domain at the very surface of the protein, it was not anticipated that disturbing this salt-bridge would influence protein structure/function to a large degree. This salt-bridge is also only moderately conserved as judged from the sequence alignment (Fig. 3). The thermostability of the K179Q mutant, however, was considerably shorter than that of the wild-type, with a half-life of less than two minutes, as compared to 53 min, at 55 °C (Table 4). The interactions between Lys^{179} and Asp^{202} and Ile^{200} connects two different helical segments of the lid domain and disruptions caused by the mutation to Gln are clearly important for maintaining a functional structure at elevated temperatures.

The effects of the K179Q mutation on enzyme function during steady state were minor. A slight increase in activity could be seen with both SO enantiomers resulting from lower K_M values and similar activities with the 2-MeSO substrates, as compared to the wild-type enzyme were also detected (Table 2). Effects on the microscopic rate constants for the reaction with (1*S*,2*S*)-2-MeSO revealed an elevated rate of alkylenzyme formation (k_2) by almost twofold to a value of 650 s^{-1}. Although the relative increase is moderate, the result suggests that an increased mobility in the lid domain favors epoxide ring opening and alkylenzyme formation. Since both catalytic Tyr residues which stabilizes the anionic alcoholate leaving group are situated in the lid domain changes in the dynamics of the protein structure are expected to influence this reaction step. In addition, the sum of the interconversion rates between ES and E′S ($k_5 + k_{-5}$) was also elevated in this mutant further indicating an increased mobility in structural elements influencing the dynamics in the enzyme–substrate complexes.

Conclusions

Disruption of intra- and inter-domain salt-bridges located away from the active-site in StEH1 cause relatively modest effects on the

overall enzyme function at moderate temperature. However, the mutations result in clear alterations to enzyme function as reflected in the kinetic parameters determined under the pre-steady state reaction phase and in the resulting regioselectivity of epoxide ring opening. The observed effects shall probably be attributed to altered dynamic properties of the enzyme structure. One indication of effects on dynamics is the severely lowered thermostability of these enzyme variants. In addition, the sum of microscopic rates of isomerizations between Michaelis complexes are in all cases increased in the mutants in the catalyzed reaction with (1*R*,2*R*)-2-MeSO, a substrate that undergoes epoxide ring opening at either carbon, further suggesting less rigid enzyme–substrate complexes. Higher rates in this isomerization step in the reaction scheme should have a direct consequence on the flux through the different pathways leading to different product diol enantiomers. This is indeed the observable results. All mutants, although K179Q to a lesser extent, display altered regioselectivity in the hydrolysis of this epoxide.

We propose that the observed alterations to regioselectivity in these mutants derive from an increased mobility in protein segments otherwise stabilized by salt bridging interactions.

Acknowledgments

This work was supported by the Swedish Research Council [Grant number 2008-3579] and The Carl Trygger Foundation [Grant number CTS 07:380].

References

[1] J. Monod, J.-P. Changeux, F. Jacob, J. Mol. Biol. 6 (1963) 306–329.
[2] G.G. Hammes, Biochemistry 41 (2002) 8221–8228.
[3] V.L. Schramm, Arch. Biochem. Biophys. 433 (2005) 13–26.
[4] P.K. Agarwal, J. Am. Chem. Soc. 127 (2005) 15248–15256.
[5] I. Bahar, C. Chennubhotla, D. Tobi, Curr. Opin. Struct. Biol. 17 (2007) 633–640.
[6] C. Frieden, Ann. Rev. Biochem. 48 (1979) 471–489.
[7] K.E. Neet, R.G. Ainslie Jr., Methods Enzymol. 64 (1980) 192–226.
[8] D. Lindberg, A. Gogoll, M. Widersten, FEBS J. 275 (2008) 6309–6320.
[9] D.L. Ollis, E. Cheah, M. Cygler, B. Dijkstra, F. Frolow, S.M. Franken, M. Harel, S.J. Remington, I. Silman, J. Schrag, J.L. Sussman, K.H.G. Verschueren, A. Goldman, Protein Eng. 5 (1992) 197–211.
[10] M. Arand, A. Cronin, F. Oesch, S.L. Mowbray, T.A. Jones, Drug. Metab. Rev. 35 (2003) 365–383.
[11] S.L. Mowbray, L.T. Elfström, K.M. Ahlgren, C.E. Andersson, M. Widersten, Protein Sci. 15 (2006) 1628–1637.
[12] A. Thomaeus, A. Naworyta, S.L. Mowbray, M. Widersten, Protein Sci. 17 (2008) 1275–1284.
[13] H.-F. Tzeng, L.T. Laughlin, S. Lin, R.N. Armstrong, J. Am. Chem. Soc. 118 (1996) 9436–9437.
[14] H.-F. Tzeng, L.T. Laughlin, R.N. Armstrong, Biochemistry 37 (1998) 2905–2911.
[15] R. Rink, J. Kingma, J.H. Lutje Spelberg, D.B. Janssen, Biochemistry 39 (2000) 5600–5613.
[16] R.N. Armstrong, C.S. Cassidy, Drug. Metab. Rev. 32 (2000) 327–338.
[17] L.T. Elfström, M. Widersten, Biochem. J. 390 (2005) 633–640.
[18] P. Masson, L.M. Schopfer, M.-T. Froment, J.-C. Debouzy, F. Nachon, E. Gillon, O. Lockridge, A. Hrabovska, B.N. Goldstein, Chem. Biol. Interact. 157–158 (2005) 143–152.
[19] A. Badiou, M.T. Froment, D. Fournier, P. Masson, L.P. Belzunces, Chem. Biol. Interact. 175 (2008) 410–412.
[20] J.D. Thompson, D.G. Higgins, T.J. Gibson, Nucleic Acids Res. 22 (1994) 4673–4680.
[21] L.T. Elfström, M. Widersten, Biochemistry 45 (2006) 205–212.
[22] M. Nardini, I.S. Ridder, H.J. Rozeboom, K.H. Kalk, R. Rink, D.B. Janssen, B.W. Dijkstra, J. Biol. Chem. 274 (1999) 14579–14586.
[23] M.A. Argiriadi, C. Morisseau, B.D. Hammock, Proc. Natl. Acad. Sci. USA 96 (1999) 10637–10642.
[24] J. Zou, B.M. Hallberg, T. Bergfors, F. Oesch, M. Arand, S.L. Mowbray, T.A. Jones, Structure 8 (2000) 111–122.
[25] G.A. Gomez, C. Morisseau, B.D. Hammock, D.W. Christianson, Biochemistry 43 (2004) 4716–4723.
[26] G.A. Gomez, C. Morisseau, B.D. Hammock, D.W. Christianson, Protein Sci. 15 (2006) 58–64.
[27] M.T. Reetz, M. Bocola, L.W. Wang, J. Sanchis, A. Cronin, M. Arand, J. Zou, A. Archelas, A.L. Bottalla, A. Naworyta, S.L. Mowbray, J. Am. Chem. Soc. 131 (2009) 7334–7343.
[28] B. van Loo, Chem. Biol. 11 (2004) 981–990.
[29] M.T. Reetz, C. Torre, A. Eipper, R. Lohmer, M. Hermes, B. Brunner, A. Maichele, M. Bocola, M. Arand, A. Cronin, Y. Genzel, A. Archelas, R. Furstoss, Org. Lett. 6 (2004) 177–180.
[30] M.T. Reetz, L.-W. Wang, M. Bocola, M. Angew, Chemie Int. Ed. 45 (2006) 1236–1241.
[31] B. van Loo, J. Kingma, G. Heyman, A. Wittenaar, J.H. Lutje Spelberg, T. Sonke, D.B. Janssen, Enzyme Microb. Technol.44 (2009) 145-153.
[32] M.I. Monterde, M. Lombard, A. Archelas, A. Cronin, M. Arand, R. Furstoss, Tetrahedron Asym. 15 (2004) 2801–2805.
[33] J.J. Tanner, R.M. Hecht, K.L. Krause, Biochemistry 35 (1996) 2597–2609.
[34] Y.-Y. Cheung, S.Y. Lam, W.-K. Chu, M.D. Allen, M. Bycroft, K.-B. Wong, Biochemistry 44 (2005) 4601–4611.
[35] G. Valentini, L. Chiarelli, R. Fortin, M.L. Speranza, A. Galizzi, A. Mattevi, J. Biol. Chem. 275 (2000) 18145–18152.
[36] R.L. Baldwin, J. Mol. Biol. 371 (2007) 283–301.
[37] S. Kumar, R. Nussinov, ChemBioChem 3 (2002) 604–617.
[38] S. Barth, M. Fischer, R.D. Schmid, J. Pleiss, Proteins Struct. Funct. Bioinf. 55 (2004) 846–855.
[39] A. Thomaeus, J. Carlsson, J. Åqvist, M. Widersten, Biochemistry 46 (2007) 2466–2479.
[40] R.E. Gawley, J. Org. Chem. 71 (2006) 2411–2416.
[41] K. Gomi, H. Yamamoto, K. Akimitsu, Plant Mol. Biol. 53 (2003) 189–199.
[42] M. Arahira, V.H. Nong, K. Udaka, C. Fukazawa, Eur. J. Biochem. 267 (2000) 2649–2657.
[43] International Rice Genome Sequencing Project, Nature 436 (2005) 793–800.
[44] L.W. Neuteboom, W.Y. Kunimitsu, D.A. Christopher, Plant Sci. 163 (2002) 1021–1035.
[45] J. Edqvist, I. Farbos, Planta 216 (2003) 403–412.
[46] T. Kiyosue, J.K. Beetham, F. Pinot, B.D. Hammock, K. Yamaguchi-Shinozaki, K. Shinozaki, Plant J. 6 (1994) 259–269.
[47] R. Velasco, A. Zharkikh, M. Troggio, D.A. Cartwright, A. Cestaro, D. Pruss, M. Pindo, L.M. FitzGerald, S. Vezzulli, J. Reid, G. Malacarne, D. Iliev, G. Coppola, B. Wardell, D. Micheletti, T. Macalma, M. Facci, J.T. Mitchell, M. Perazzolli, G. Eldredge, P. Gatto, R. Oyzerski, M. Moretto, N. Gutin, M. Stefanini, Y. Chen, C. Segala, C. Davenport, L. Dematte, A. Mraz, J. Battilana, K. Stormo, F. Costa, Q. Tao, A. Si-Ammour, T. Harkins, A. Lackey, C. Perbost, B. Taillon, A. Stella, V. Solovyev, J.A. Fawcett, L. Sterck, K. Vandepoele, S.M. Grando, S. Toppo, C. Moser, J. Lanchbury, R. Bogden, M. Skolnick, V. Sgaramella, S.K. Bhatnagar, P. Fontana, A. Gutin, Y. Van de Peer, F. Salamini, R. Viola, PLoS ONE 2 (2007) e1326.